

Article

Enhanced Salp Swarm Algorithm for Multimodal Optimization and Fuzzy Based Grid Frequency Controller Design

Smrutiranjan Nayak¹, Sanjeeb Kumar Kar¹, Subhransu Sekhar Dash², Pradeep Vishnuram³ ,
Sudhakar Babu Thanikanti⁴  and Benedetto Nastasi^{5,*} 

- ¹ Department of Electrical Engineering, ITER, Siksha 'o' Anusandhan (Deemed to Be University), Bhubaneswar 751030, India; smrutikiit40@gmail.com (S.N.); sanjeebkar@soa.ac.in (S.K.K.)
- ² Department of Electrical Engineering, Government College of Engineering, Keonjhar 758002, India; subhransudash_fee@gcekjr.ac.in
- ³ Department of Electrical and Electronics Engineering, SRM Institute of Science and Technology, Chennai 603203, India; pradeep.kannan03@gmail.com
- ⁴ Department of Electrical and Electronics Engineering, Chaitanya Bharathi Institute of Technology, Hyderabad 500075, India; sudhakarbabu@ieee.org
- ⁵ Department of Planning, Design, and Technology of Architecture, Sapienza University of Rome, Via Flaminia 72, 00196 Rome, Italy
- * Correspondence: benedetto.nastasi@outlook.com

Abstract: In the present study, an Enhanced SSA (ESSA) has been proposed where the parameter of the SSA technique, which balances the exploration and exploitation phases, has been modified. Additionally, the variable scaling factor is engaged to regulate the salp's position during the search procedure to minimize the random movement of salps. To demonstrate the effectiveness of the enhanced SSA (ESSA), a set of multimodal test functions are engaged. The statistical outcomes demonstrate that ESSA profits from local optima evasion and quick convergence speed, which aids the proposed ESSA algorithm to outclass the standard SSA and other recent algorithms. The fair analysis displays that ESSA delivers very promising results and outclass current methods. Next, frequency control of power systems is executed by designing a Combined Fuzzy PID (CFPID) controller with the projected ESSA method. Next, a Partially Distributed CPFID (PD-CFPID) controller is designed for a distributed power system (DPS). It is shown that the ESSA method outclasses the SSA method in engineering problems. It is also noted that the ESSA-based PD-CFPID scheme has become more operative in monitoring the frequency than similar structured centralized fuzzy PID (CFPID) as well as PID controller. Finally, the outcomes of the PD-CFPID controller are equated with CFPID and PID for various uncertain situations to validate the benefit of the proposed control approach.

Keywords: salp swarm algorithm (SSA); frequency control; partially decentralized combined fuzzy PID; distributed power system



Citation: Nayak, S.; Kar, S.K.; Dash, S.S.; Vishnuram, P.; Thanikanti, S.B.; Nastasi, B. Enhanced Salp Swarm Algorithm for Multimodal Optimization and Fuzzy Based Grid Frequency Controller Design. *Energies* **2022**, *15*, 3210. <https://doi.org/10.3390/en15093210>

Academic Editor: Eduard Petlenkov

Received: 13 March 2022

Accepted: 25 April 2022

Published: 27 April 2022

Publisher's Note: MDPI stays neutral with regard to jurisdictional claims in published maps and institutional affiliations.



Copyright: © 2022 by the authors. Licensee MDPI, Basel, Switzerland. This article is an open access article distributed under the terms and conditions of the Creative Commons Attribution (CC BY) license (<https://creativecommons.org/licenses/by/4.0/>).

1. Introduction

With the growing count of irregular renewable and distributed energies in the presence of random load changes, today's power systems are vulnerable to frequency variations [1,2]. Therefore, a suitable controller is required for frequency regulation. The distributed control approach has multiple distributed controllers for each controllable energy source located within the distributed power system (DPS) [3]. However, the distributed control approach requires one-to-one communication between each controllable source. Complete control requirements such as matching collective load and generation or optimum generation combination are not usually achievable with a distributed control scheme. Hence, if system optimization is the objective, a centralized control scheme is generally favored [4]. In a centralized control scheme, all control requirements are handled by a central computer [5]. While centralized approaches frequently suffer if there is a single failure,

decentralized schemes are usually associated with difficult practical implementations and costly communication requirements. Considering the shortcomings of both centralized and decentralized control schemes, this paper proposes to use a partially decentralized controller for the frequency regulation of DPS. The proposed partially decentralized control scheme, which compared with the decentralized control can take the coupling information into account, thus enhancing the system performance without making the design process too complicated.

The controller design is again a tough job and numerous methods have been suggested by researchers in this regard. The salp swarm algorithm (SSA) is a recently proposed process encouraged by the swarming conduct of the salps [6]. The advantage of the SSA method over some similar methods such as the firefly algorithm (FA), bat algorithm (BA), state of matter search (SMS), flower pollination algorithm (FPA), particle swarm optimization (PSO), gravitational search algorithm (GSA), and genetic algorithm (GA) has been testified [6]. The SSA algorithm keeps the best results found so far, therefore SSA is unaffected even if the entire populations worsen. In SSA, salps move gradually towards the leading salp, which prevents stagnating in local minima. The parameter $c1$ is reduced adaptively during iterations, so the algorithm initially explores and then exploits the search area. The above characteristics enable SSA to outperform other algorithms. However, the original SSA method hurts from early convergence, therefore making it inappropriate for multimodal function optimization problems such as controller design problems. In the SSA method, the convergence parameter ($c1$) is changed gradually in the early phases of iterations and rapidly in the closing phases, which lowers the exploration competence of the process. In the projected enhanced SSA (ESSA) method, the algorithm is altered to conquer the limitations of the SSA method. Additionally, in the SSA, the location of the supporter salp is calculated from its previous location and surrounded by the salp's location. The equation for finding the location of follower salp is also altered by means of varied scaling factors to avoid the random movement of salps.

Different heuristic-based optimization methods have been used to determine the values of controller parameters for frequency control approaches as shown in Table 1. The table explains the technique, controller type, test system, and the limitations of the frequency control approach used for various test systems.

Table 1. Comparative analysis of various frequency control approaches in different test systems.

Ref. No.	Optimization Technique and Controller	Test System	Remarks
[7]	Quasi oppositional Jaya (QOJAYA) tuned two-degree of freedom (2DOF) PID controller	Two area power systems consist of the thermal and hydropower plants including the nonlinearities.	QOJAYA may not be effective for the systems containing several peaks and trapped in local minima due to its single oppositional-based approach. 2DOF PID controller may not be effective in presence of nonlinearity and uncertainties.
[8]	Sine logistic map based chaotic sine cosine algorithm tuned PID	Islanded microgrid with PV, wind, Fuel Cell, BESS, FESS, DEG, and MT	Time delay and uncertain cases are not considered. The PID controller may not offer effectual control for nonlinear, uncertain systems and in presence of time delay and unstable transfer functions. Centralized PID controller performance may degrade in presence of nonlinearity and uncertainties.
[9]	Intelligent model predictive control	Microgrid with PV, wind, Fuel Cell, BESS, FESS, DEG, and MT with electric vehicle	Time delay and uncertain cases are not considered. Model predictive control approaches have difficulties with the operation, high maintenance cost, and lack of flexibility resulting in fragile controllers that are not profitable.
[10]	2DOF-tilted integral derivative with filter tuned by bat and harmony search algorithm	Two-area wind-hydro-diesel units with SMES and FACTS devices	Time delay and uncertain cases are not considered. In the 2DOF PID controller, the tuning for the disturbance and the set-point response are not often compatible. Centralized 2DOF-TID performance may degrade in presence of nonlinearity and uncertainties.

Table 1. Cont.

Ref. No.	Optimization Technique and Controller	Test System	Remarks
[11]	Proportional-derivative with filter cascaded-proportional-integral tuned by the coyote optimization algorithm	Two-area power system with photovoltaic (PV) and wind farm and gas turbine interconnection	The effectiveness of the optimization technique has not been tested in benchmark test functions. Time delay is not considered. Variants of PID controllers are suitable for linear systems and incompatible for nonlinear systems.
[12]	Chaotic atom search optimization based fractional-order PID controller	Multi-area hybrid power system consisting of thermal, hydro, gas, solar-thermal, wind, and aqua electrolyzer-fuel cell	Sever uncertainties such as unavailability of some sources and communication delays are not considered. Decentralized FO PID controllers have difficult practical implementations and costly communication requirements.
[13]	Sailfish optimizer (SFO) optimized fuzzy tilt integral derivative controller	Microgrid containing DEG, PV, FC, AE, BESS, FESS, and FESS	In SHO, the combination may create prey extra prominent to predators and may amplify intra-specific rivalry. Additionally, those in the preferred central locations may have inferior feeding rates. A centralized control scheme may cause a problem in case of a single failure.
[14]	Mayfly optimization-based fuzzy PD-(1 + I) controller	Interconnected microgrid containing Solar-thermal, Wind, Micro-hydro turbine, Biodiesel, and Biogas generators.	In the MO method, if the present locations were away from the best locations, slower convergence may occur. A centralized Fuzzy PD-(1 + I) control scheme is inferior to a decentralized scheme and may cause a problem in case of a single failure.
[15]	Direct synthesis (DS) method based fractional order PID controller	Reheat thermal, hydropower, and non-reheat thermal IEEE 39-bus New England IEEE 39-bus test system along with variable communication delay.	The direct synthesis (DS) approach depends on the process model. The overshoots and undershoots in transient response may be high and fine-tuning may be required. The study is limited to conventional generating units. PID controllers are not suitable for nonlinear and uncertain systems.
[16]	Atom search optimization-based FOPID controller	Two area hybrid power systems containing PEV, WTPG, STPG, and thermal units consider nonlinearities.	In ASO, a small variation in velocities causes inferior exploitation in the later stages of the algorithm. FOPID controllers are not suitable for nonlinear and uncertain systems.
[17]	Grey wolf optimization (GWO) based FOPID controller	A hybrid power system containing PEV, WTG, PV, and DEG with Energy storage elements.	The GWO method calculates the wolves' positions by the mean locations, ignoring the wolf ladder, which may lead GWO to local convergence. FOPID controllers are not suitable for nonlinear and uncertain systems.
[18]	Ant lion optimizer (ALO) based FOPID controller	Two area systems containing conventional and renewables	The arbitrary walking method in ALO results in a large run time. FOPID controllers are not suitable for nonlinear and uncertain systems.
[19]	Particle swarm optimization-based Fuzzy PI controller	Thermal generator with BESS including the effect of demand response	PSO has poor exploration capability with a large execution time for complex systems. Decentralized FO PID controllers have difficult practical implementations and costly communication requirements.
[20]	Archimedes optimization algorithm tuned integral derivative-tilted (ID-T) controller,	Two area systems containing conventional and renewables units.	AOA is not resistant to the unequal exploration and exploitation stages leading to local optimum. A system with a centralized ID-T controller will collapse in case of a single failure.
[21]	Marine predators algorithm (MPA) tuned PID controller	Two-area system containing conventional and renewable energy sources (wind, PV, and STPP) and energy storing units (SMES and BES)	The disadvantages of the MPA are failure to create a diverse early population, local minima avoidance, and poor exploration. PID controllers are not suitable for nonlinear and uncertain systems.
[22]	Adaptive-neuro-fuzzy inference system (ANFIS) based controller	Single area and two-area hydropower plants.	ANFIS applications in problems with large inputs are computationally expensive. ANFIS controller is complex and requires the expert user to handle.
[23]	Artificial bee colony (ABC) based PID fuzzy logic controller	Fourteen generations Australian test system with wind and battery integration.	ABC suffers from improper exploitation in solving complicated problems. The controller is not adaptive to handle uncertainties.

The chief contributions of the study are:

- i. To develop an enhanced SSA (ESSA) process and authenticate its effectiveness over original SSA and other similar algorithms [24–33] using 16 multimodal test functions of different dimensions.
- ii. To design a combined fuzzy PID (CFPID) for frequency control in two area systems and compare its performance with similar approaches reported in the literature.
- iii. To design a partially decentralized combined fuzzy PID (PD-CFPID) controller for frequency regulation of a hybrid power system containing PV, DEG, WTG, with energy storage elements such as FESS, AE, FC, BES, and EV considering the inherent nonlinearities and communication delays.
- iv. To assess the efficacy of ESSA based PD-CFPID under the following uncertain scenarios:
 - Scenario A:* P_{WTG} , P_{PV} , and P_D are augmented by 200%;
 - Scenario B:* P_{WTG} and P_{PV} are unavailable but the P_D is augmented by 200%;
 - Scenario C:* EV power and load demand pattern are augmented by 100% and 200%, respectively;
 - Scenario D:* P_{WTG} and P_{PV} are decreased by 50% but P_{EV} and P_D are augmented by 100% and 200%, respectively;
 - Scenario E:* The time delay is enhanced to 400 ms.

2. Overview of Enhanced Salp Swarm Algorithm (ESSA)

The main inspiration of the salp swarm method is the spilling over the behavior of the principal swarms on the earth [6]. The whole inhabitants of salp are separated into leader and followers' groups. The best location of the salp order is taken by the leader and guides the remaining swarms. The remaining salps trail the leader. The location of the salp is categorized by an n -dimensional search area. The food resource T is the aim for the salp in the pursuit search.

The position of the leader is given by Equation (1) as

$$x_j^1 = \begin{cases} T_j + c_1((ub_j - lb_j)c_2 + lb_j) & c_3 \geq 0.5 \\ T_j - c_1((ub_j - lb_j)c_2 + lb_j) & c_3 \leq 0.5 \end{cases} \quad (1)$$

where x_j^1 and T_j represent the locations of the leader and food source in the j -th dimension. The leader changes its place concerning the food resource only. The bounds of j -th dimension are specified by lb_j, ub_j . The parameter c_2 and c_3 are arbitrary values in $[0, 1]$. The coefficient c_1 equilibrates the exploration and exploitation stages of the SSA method.

It is represented as

$$c_1 = K_1 \exp \left[- \left(\frac{4i_c}{I_M} \right)^2 \right] \quad (2)$$

where i_c and I_M signifies the current and the maximum iterations and K_1 is a constant which is set as 2 in SSA.

The location of the remaining salps is restructured by

$$x_j^i = \frac{1}{2}at^2 + v_0t \quad (3)$$

Equation (3) corresponds to Newton's law of motion where $i \geq 2$, t signifies time, v_0 which means the original speed. These are calculated as: $a = \frac{v_{final}}{v_0}$ and $v_0 = \frac{x-x_0}{t}$. Considering $v_0 = 0$ that variance amid iterations is equal to 1, then Equation (3) is altered as,

$$x_j^i = \frac{(x_j^i + x_j^{i-1})}{2} \quad i \geq 2 \quad (4)$$

where x_j^i signifies the position of the i -th follower in j -th dimension.

In the proposed ESSA procedure, two SSA parameters were altered for better symmetry between the exploration and exploitation stages. A balance between the two enhances the process. The occasion of the leader is a vital aspect of the SSA process which is eventually guided by parameters c_1 . The value of K_1 is taken as 2 in the SSA process which administrates the movement of the leader salp associated to T . An large K_1 may cause salp stirring outside the food source location. In ESSA process K_1 is varied to make the spreading of searched arguments near the best than the initial argument. In SSA, c_1 changes gradually linearly iterations and quickly in later stages. If c_1 is set higher values in the latter stages, it will make the method produce a greater aberration of the leader's location. These glitches are also quashed in ESSA with the adapted value of K_1 by randomly changing to a lesser c_1 value in the final phases as:

$$K_1 = \begin{cases} 2(1 - i_c/I_M) & \text{if } randm < 0.5 \\ 2 & \text{if } randm \geq 0.5 \end{cases} \quad (5)$$

The position of the follower salp in the original SSA is expressed as:

$$x_j^i = 1/2 (x_j^i + x_j^{i-1}) \quad i \geq 2 \quad (6)$$

where x_j^i and x_j^{i-1} are the positions of i -th and $(i - 1)$ -th salps in j -th dimension. In the early stages, the finest probable search agent is unidentified in the search area. Therefore, the procedure of updating in huge steps firstly will result in stirring salps missing the best locations. Thus, the usage of scaling factors (SF) in ESSA regulates the advancement of search agents during the search procedure. The new equation is formulated as:

$$x_j^i = SF \cdot \left[1/2 (x_j^i + x_j^{i-1}) \right] \quad i \geq 2 \quad (7)$$

where SF is varied linearly from 0.1 to 1 as expressed in Equation (8):

$$SF = 1 / (10 - 9 \frac{i_c}{I_M}) \quad (8)$$

The inclusion of SF adjusts the drive of saps in the early stages of the method, thus augmenting the search competence of the algorithm. In the advanced phases, as improved solutions are found, salps move in the direction of them at progressively increased speed.

3. Performance Study of ESSA Technique

In this study, the engineering application is a controller design problem. Tuning the controller parameter is a highly nonlinear and complex multimodal optimization problem as many settings of the controller could yield satisfactory performance. As the application area of the present study is the controller design problem, i.e., multimodal optimization problem, therefore benchmark multimodal test functions are used to evaluate the performance of the proposed ESSA technique.

The proposed ESSA is verified on some multimodal functions [34,35] and given in Table 2. Multi-modal functions (*mmf*) 1 to 6 are of 10 dimensions and 7 to 16 are of different fixed dimensions. To authenticate the efficacy of the suggested ESSA algorithm it is equated with SSA as well as with WCMFO [24], ABC [25], GA [26], CamWOA [27], PSO [28], GSA [29], PSOGSA [30], WCA [31], MFO algorithm [32] and DA [33] as given in [24,27]. The no. of function estimations is set as 100,000 for all approaches for an unbiased assessment. In ESSA, 1000 iterations with 100 no. of search agents are considered. The parameters of all the techniques are taken from reference [24,27]. The statical outcomes found in 30 runs are assembled. For the appropriate selection of SF , several equations are tried and evaluated. It is realized that for the many functions best outcomes are found when SF is found by Equation (8) as related to others.

Table 2. Multimodal functions.

Function Name	Expression	Range	Dim.	Opt.
Generalized Schwefel	$mmf_1(y) = \sum_{i=1}^n -y_i \sin(\sqrt{ y_i })$	[-500, 500]	10	-2094.9145
Generalized Rastrigin	$mmf_2(y) = \sum_{i=1}^n [y_i^2 - 10 \cos(2\pi y_i) + 10]$	[-5.12, 5.12]	10	0
Ackley	$mmf_3(y) = -20 \exp \left(-0.2 \sqrt{\frac{1}{n} \sum_{i=1}^n y_i^2} \right) - \exp \left(\frac{1}{n} \sum_{i=1}^n \cos(2\pi y_i) \right) + 20$	[-32, 32]	10	0
Generalized Griewank	$mmf_4(y) = \frac{1}{4000} \sum_{i=1}^n y_i^2 - \prod_{j=1}^n \cos\left(\frac{y_j}{\sqrt{j}}\right) + 1$	[-600, 600]	10	0
Generalized Penalized Function 1	$mmf_5(y) = \frac{\pi}{n} \{10 \sin \sin(\pi x_i) + \sum_{i=1}^{n-1} (y_i - 1)^2 [1 + 10 \sin^2(\pi x_{i+1})]\} + (x_n - 1)^2 + \sum_{i=1}^n u(y_i, 10, 100, 4)$ $x_i = 1 + \frac{y_i + 1}{4}$ $u(y_i, a, k, m) = \begin{cases} k(y_i - a)^m y_i & > a \\ 0 & -a < y_i < a \\ k(-y_i - a)^m y_i & < -a \end{cases}$	[-50, 50]	10	0
Generalized Penalized Function 2	$mmf_6(y) = 0.1 \left\{ \sin^2 + \sum_{i=1}^n (y_i - 1)^2 [1 + \sin^2(3\pi y_i + 1)] + (y_n - 1)^2 [1 + \sin^2(2\pi y_n)] \right\} + \sum_{i=1}^n u(y_i, 5, 100, 4)$	[-50, 50]	10	0
Shekel's Foxholes	$mmf_7(y) = \left(\frac{1}{500} + \sum_{j=1}^{25} \frac{1}{j + \sum_{i=1}^2 (y_i - a_{ij})^2} \right)^{-1}$	[-65.536, -65.536]	2	1
Kowalik	$mmf_8(y) = \sum_{i=1}^{11} \left[a_i - \frac{y_1 (b_i^2 + b_i y_2)}{b_i^2 + b_i y_3 + y_4} \right]^2$	[-5, 5]	4	0.0003
Six-Hump Camel-Back	$mmf_9(y) = 4y_1^2 - 2.1y_1^4 + \frac{1}{3}y_1^6 + y_1 y_2 - 4y_2^2 + 4y_2^4$	[-5, 5]	2	-1.0316
Branin	$mmf_{10}(y) = \left(y_2 - \frac{5.1}{4\pi^2} y_1^2 + \frac{5}{\pi} y_1 - 6 \right)^2 + 10 \left(1 - \frac{1}{8\pi} \right) \cos(y_1) + 10$	[-5, 10] [0, 15]	2	0.398
Goldstein-Price	$mmf_{11}(y) = [1 + (y_1 + y_2 + 1)^2 (19 - 14y_1 + 3y_1^2 - 14y_2 + 6y_1 y_2 + 3y_2^2)] \times [30 + (2y_1 - 3y_2)^2 \times (18 - 32y_1 + 12y_1^2 + 48y_2 - 36y_1 y_2 + 27y_2^2)]$	[-2, 2]	2	3
Hartman's 1	$mmf_{12}(y) = - \sum_{i=1}^4 c_i \exp \left(- \sum_{j=1}^3 a_{ij} (y_j - p_{ij})^2 \right)$	[0, 1]	3	-3.86
Hartman's 2	$mmf_{13}(y) = - \sum_{i=1}^4 c_i \exp \left(- \sum_{j=1}^6 a_{ij} (y_j - p_{ij})^2 \right)$	[0, 1]	6	-3.32
Shekel's 1	$mmf_{14}(y) = - \sum_{i=1}^5 [(Y - a_i)(Y - a_i)^T + c_i]^{-1}$	[0, 10]	4	-10.1532
Shekel's 2	$mmf_{15}(y) = - \sum_{i=1}^7 [(Y - a_i)(Y - a_i)^T + c_i]^{-1}$	[0, 10]	4	-10.4028
Shekel's 3	$mmf_{16}(y) = - \sum_{i=1}^{10} [(Y - a_i)(Y - a_i)^T + c_i]^{-1}$	[0, 10]	4	-10.5363

The statistical result of ESSA and SSA obtained along with the outcomes of the other 10 methods available in reference [24,27] are presented in Tables 3 and 4 for 10 dimensions and fixed dimensions $mmfs'$, respectively. It can be noticed from Tables 3 and 4 that suggested ESSA outperforms original SSA in 15 out of 16 $mmfs'$ (except $mmf_6(y)$). It can also be realized from Table 3 that ESSA outperforms all other 11 techniques in the majority of functions (in 3 out of 6 $mmfs'$). For fixed dimension multimodal functions, the proposed ESSA provides an optimum of equally best results in 9 out of 10 $mmfs'$ as evident from Table 4.

Table 3. Statistical results for 10 dimension functions.

Function	ESSA		SSA		GA		PSO	
	Av.	St.Dev	Av.	St.Dev	Av.	St.Dev	Av.	St.Dev
<i>mmf</i> _{1y}	−2796.049	3349.21	−2930.15	3099.72	−3692.39	182.42	−2742.78	274.7175
<i>mmf</i> _{2y}	0	0	11.8731	3.7767	3.8E−4	3.2E−4	1.757	1.1592
<i>mmf</i> _{3y}	8.88E−16	0	0.2089	0.4824	8.88E−16	1.0E−31	8.88E−16	1.00E−31
<i>mmf</i> _{4y}	3.29E−14	1.897E−14	0.268906	0.14071	5.6E−2	3E−2	0.1244	8.04E−2
<i>mmf</i> _{5y}	3.501E−16	2.437E−16	0.09329	0.16637	5.73E−05	1.4E−4	4.71E−32	1.67E−47
<i>mmf</i> _{6y}	1.829E−15	1.456E−15	1.831E−3	4.164E−3	6.21E−05	1.1E−4	1.34E−32	5.56E−48
Function	DA		WCA		GSA		MFO	
	Av.	St.Dev	Av.	St.Dev	Av.	St.Dev	Av.	St.Dev
<i>mmf</i> _{1y}	−3213.66	431.748	−3422.55	304.572	−1694.53	190.6721	−3329.13	288.317
<i>mmf</i> _{2y}	11.561	10.177	20.993	10.524	1.392	1.214	12.8372	7.352
<i>mmf</i> _{3y}	3.14E−05	1.7E−04	2.42E−15	1.79E−15	1.28E−10	6.71E−11	8.88E−16	1.00E−31
<i>mmf</i> _{4y}	0.3846	0.3826	0.1502	9.44E−2	1.67E−2	2.79E−2	1.78E−01	8.43E−02
<i>mmf</i> _{5y}	0.5296	0.6912	1.036E−2	5.67E−2	7.95E−21	3.23E−21	3.11E−02	9.487E2
<i>mmf</i> _{6y}	0.5292	0.7173	7.3E−4	2.7E−3	5.67E−20	1.88E−20	1.10E−3	3.33E−3
Function	CS		PSO_GSA		ABC		WCMFO	
	Av.	St.Dev	Av.	St.Dev	Av.	St.Dev	Av.	St.Dev
<i>mmf</i> _{1y}	−3712.01	167.4447	−3271.6	278.08	−3922.73	88.61857	−3729.7	96.325
<i>mmf</i> _{2y}	6.574	1.367	23.281	12.968	3.677	1.0365	2.089	1.508
<i>mmf</i> _{3y}	1.24E−15	1.08E−15	4.94E−12	2.26E−12	1.21E−06	9.37E−07	8.88E−16	1.00E−31
<i>mmf</i> _{4y}	3.96E−02	8.8E−3	0.2004	0.1141	0.281	0.1086	9.91E−02	5.31E−2
<i>mmf</i> _{5y}	9.77E−05	1.3E−4	0.2491	0.581	1.9E−3	1.3E−3	2.00E−29	6.44E−29
<i>mmf</i> _{6(y)}	1.31E−09	1.39E−09	3.11E−21	1.06E−21	8.3E−3	5.1E−3	4.49E−22	2.06E−21

Table 4. Statistical results for fixed dimensional functions.

Function	ESSA		SSA		GA		PSO	
	Av.	St.Dev	Av.	St.Dev	Av.	St.Dev	Av.	St.Dev
<i>mmf</i> _{7y}	0.998	0	0.998	0	0.998	8.83E−14	1.56	0.959
<i>mmf</i> _{8y}	3.421E−4	1.678E−4	8.863E−4	3.397E−4	8.4E−4	2.9E−4	7E−4	3.2E−4
<i>mmf</i> _{9y}	−1.0316	0	−1.0316	0	−1.03	5.02E−10	−1.03	3
<i>mmf</i> _{10y}	3.98E−1	8E−17	3.98E−1	4.0E−16	3.98E−1	4.73E−7	3.98E−1	1.13E−16
<i>mmf</i> _{11y}	3	4.054E−14	3	4.3E−14	3	1.21E−8	3	4.52E−16
<i>mmf</i> _{12y}	−3.86	2.14E−15	−3.86	5E−15	−3.86	2.203E−3	−3.86	2.7E−15
<i>mmf</i> _{13y}	−3.2504	3.017E−2	−3.25	6.001E−3	−3.32	2.170E−2	−3.26	6.04E−2
<i>mmf</i> _{14y}	−10.1532	5E−14	−9.7342	1.6244	−10.2	0.00048	−9.31	1.9255
<i>mmf</i> _{15y}	−10.4029	2.14E−11	−10.2271	0.9629	−9.93	1.822	−9.52	2.00228
<i>mmf</i> _{16y}	−10.5364	4E−15	−10.5364	4E−15	−9.61	2.405	−10	1.6357

Table 4. Cont.

Function	DA		WCA		GSA		MFO	
	Av.	St.Dev	Av.	St.Dev	Av.	St.Dev	Av.	St.Dev
<i>mmf</i> _{7y}	1.1	0.303	0.998	3.39E−16	3.4	2.578637	1.03	0.181483
<i>mmf</i> _{8y}	1.34E−3	5.11E−4	3.69E−4	2.32E−4	1.8E−3	4.9E−4	8.37E−4	2.54E−4
<i>mmf</i> _{9y}	−1.03	2.55E−11	−1.03	0	−1.03	0	−1.03	0
<i>mmf</i> _{10y}	3.98E−1	7.6E−13	3.98E−1	3.79E−16	3.98E−1	1.13E−16	3.98E−1	1.13E−16
<i>mmf</i> _{11y}	3	1.38E−6	3	1.79E−14	3	4.02E−15	3	1.95E−15
<i>mmf</i> _{12y}	−3.86	1.587E−03	−3.86	2.71E−15	−3.86	2.71E−15	−3.86	2.71E−15
<i>mmf</i> _{13y}	−3.25	6.72E−02	−3.26	6.04E−2	−3.32	1.36E−15	−3.22	4.5066E−2
<i>mmf</i> _{14y}	−9.81	1.28	−8.31	2.718	−7.45	3.381188	−7.56	3.323037
<i>mmf</i> _{15y}	−10.4	0.192	−9.52	2.002	−10.4	0	−9.35	2.423664
<i>mmf</i> _{16y}	−10.3	1.06	−9.82	2.235	−10.5	9.03E−15	−10.3	1.39948
Function	CS		PSOGSA		ABC		WCMFO	
	Av.	St.Dev	Av.	St.Dev	Av.	St.Dev	Av.	St.Dev
<i>mmf</i> _{7y}	0.998	3.39E−16	1.06	0.252	0.998	1.02E−13	0.998	5.36E−16
<i>mmf</i> _{8y}	3E−4	4.23E−9	3.79E−3	7.5E−3	7E−4	1.3E−4	3.0E−4	1.07E−15
<i>mmf</i> _{9y}	−1.03	0	−1.03	0	−1.03	7.36E−11	−1.03	0
<i>mmf</i> _{10y}	3.98E−1	1.13E−16	3.98E−1	1.13E−16	3.98E−1	5.68E−09	3.98E−1	1.13E−16
<i>mmf</i> _{11y}	3	4.52E−16	3	4.52E−16	3	8.64E−05	3	9.57E−15
<i>mmf</i> _{12y}	−3.86	2.71E−15	−3.86	2.71E−15	−3.86	7.89E−11	−3.86	2.71E−15
<i>mmf</i> _{13y}	−3.32	1.26E−13	−3.26	6.032E−2	−3.32	4.82E−06	−3.25	6.027E−2
<i>mmf</i> _{14y}	−10.2	1.81E−15	−5.9	3.421068	−10.1	6.784E−3	−8.89	2.361515
<i>mmf</i> _{15y}	−10.4	6.18E−14	−5.76	3.454976	−10.4	2.886E−3	−10.4	1.59E−12
<i>mmf</i> _{16(y)}	−10.5	2.15E−12	−6.99	3.890193	−10.5	4.074E−3	−10.5	4.09E−14

Convergence figures for ESSA and SSA are related in Figure 1 for some *mmfs'* from which it can be noticed that the convergence feature of ESSA is improved. This is because of modifying the value K_1 by randomly changing to a lower value C_1 during the latter stages of iteration and the use of *SF* to restrict the drive of saps in the initial periods of the search process. It is worthwhile to mention here that for *mmf*₁, typical ESSA converges near to the best value of −2094.9145. Similarly, for *mmf*₃ and *mmf*₁₄ even though both ESSA and SSA converge to the same value, ESSA converges faster compared to SSA.

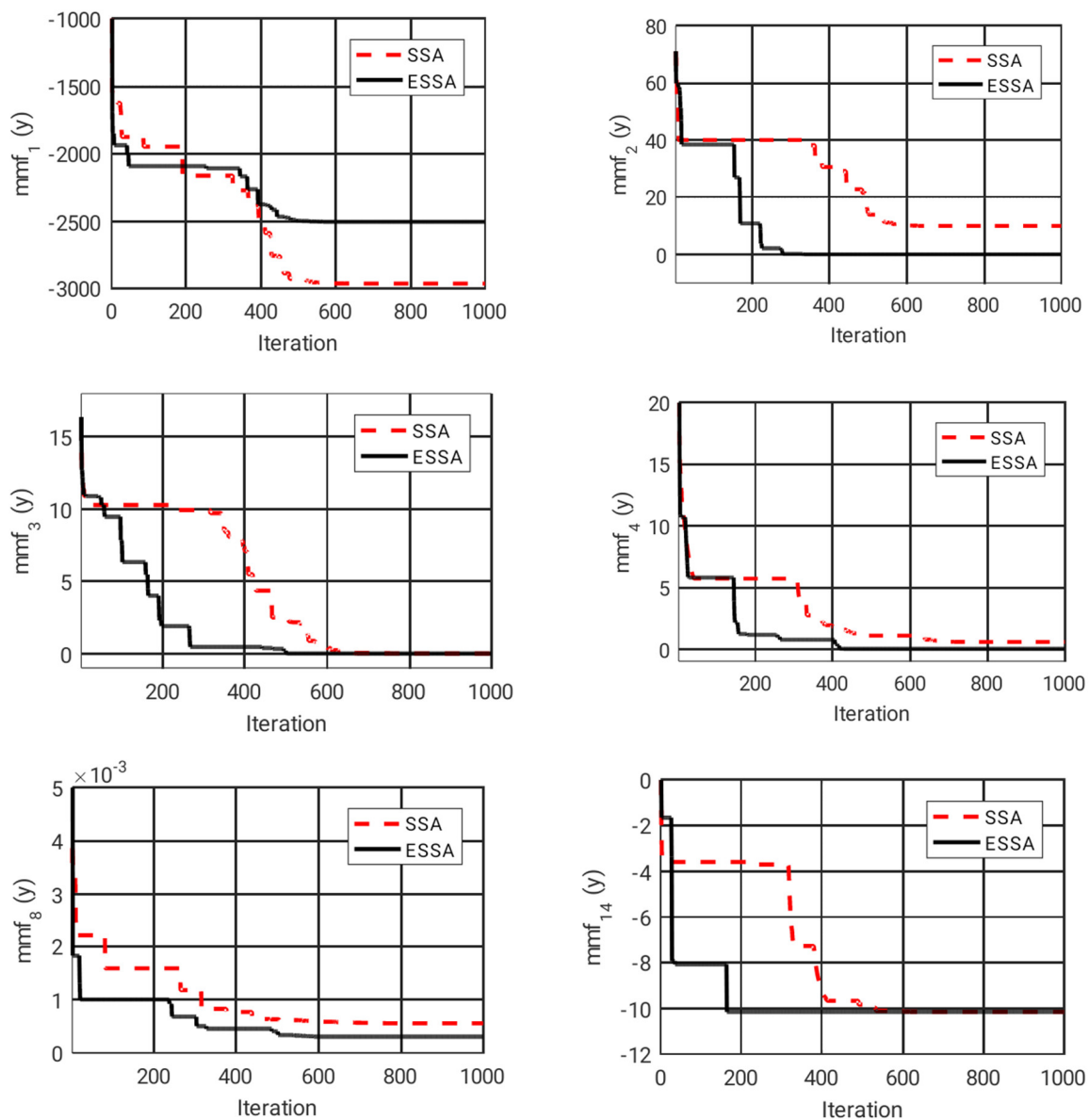


Figure 1. Convergence curves with SSA and ESSA for some $mmfs$.

4. Proposed Frequency Control Approach

The proposed ESSA method is applied and tried for frequency regulation of hybrid power system (HPS) as shown in Figure 2. It contains PV, WTG FC, DEG, AE, BESS, FESS, and electric vehicles, etc. [4,36–39]. The performance of HPS in the presence of wind and solar generation is extremely erratic and therefore the power balance is a complex task. Hence this problem can be resolved by appropriate management among stability and controllability. In this study, a partially decentralized controller is engaged, which makes it a modest control and requires less maintenance as well as dealing with fewer controllable parameters. Limiters are involved in each component to match fluctuations in the electromechanical features of the specific subsystem. In addition, time delays associated with input/output to the controller (10 ms) are considered. In Figure 2, the control participation factors (CPF) of controllable sources such as DEG, FESS, BESS, and EV are represented by corresponding CPFs.

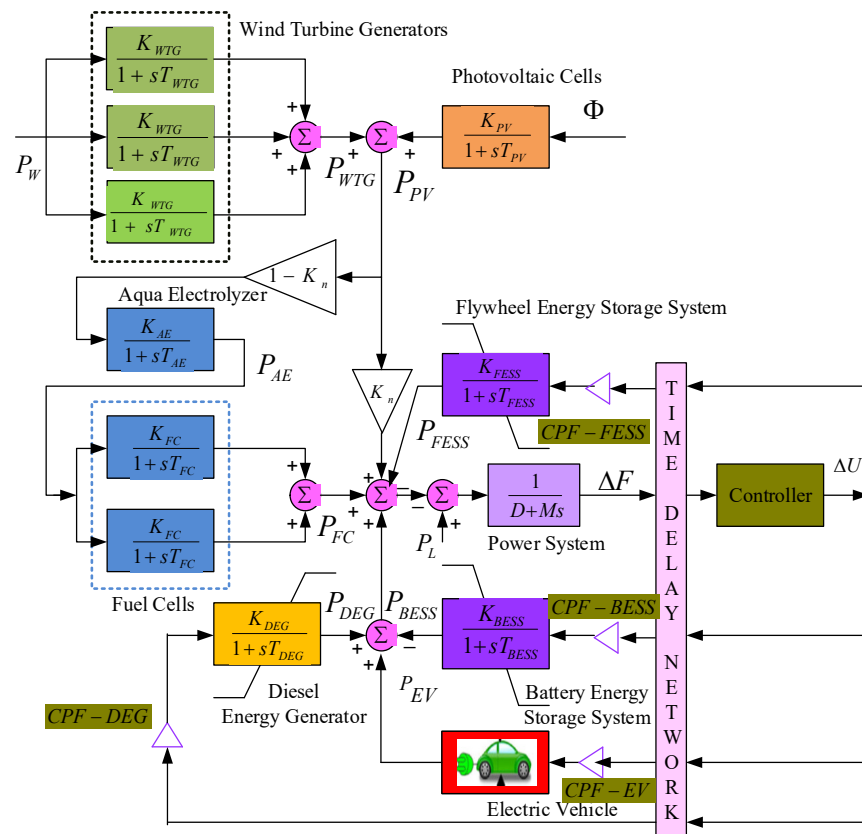


Figure 2. Studied Hybrid power system.

4.1. Modelling of Parts

4.1.1. Wind Turbine Generator (WTG)

The WTG power output is assumed as [5]:

$$P_{WP} = \frac{1}{2} \rho A_R C_P V_W^3 \tag{9}$$

The transfer function (TF) of WTG is

$$G_{WTG_N}(s) = \frac{K_{WTG}}{1 + sT_{WTG}} = \frac{\Delta P_{WTG}}{\Delta P_{WP}} \tag{10}$$

where $N = 1, 2, 3$.

4.1.2. Photovoltaic Cell (PV)

PV power output is assumed as [5]

$$P_{PV} = \eta \cdot S \cdot \phi [1 - 0.005(T_a + 25)] \tag{11}$$

where η is the conversion efficiency of PV cells and taken as 10%, S is the area of PV array taken as 4084 m² and ϕ is the solar irradiation in kW/m². A PV TF is assumed as [5]

$$G_{PV}(s) = \frac{K_{PV}}{1 + sT_{PV}} = \frac{\Delta P_{PV}}{\Delta \phi} \tag{12}$$

4.1.3. Aqua Electrolyzer

Aqua electrolyzer receives a majority of the total power from renewable sources. The AETF is stated as [5]

$$G_{AE}(s) = \frac{K_{AE}}{1 + sT_{AE}} = \frac{\Delta P_{AE}}{U_2} \quad (13)$$

4.1.4. Fuel Cell

The TF of FC is assumed as

$$G_{FCN}(s) = \frac{K_{FC}}{1 + sT_{FC}} = \frac{\Delta P_{FC}}{\Delta P_{AE}} \quad (14)$$

where $N = 1, 2$.

4.1.5. Diesel Engine Generator (DEG)

The TF of DEG is assumed as

$$G_{DEG}(s) = \frac{K_{DEG}}{1 + sT_{DEG}} = \frac{\Delta P_{DEG}}{\Delta U} \quad (15)$$

4.1.6. FESS and BESS

The TF of FESS and BESS are [5]

$$G_{FESS}(s) = \frac{K_{FESS}}{1 + sT_{FESS}} = \frac{\Delta P_{FESS}}{\Delta U} \quad (16)$$

$$G_{BESS}(s) = \frac{K_{BESS}}{1 + sT_{BESS}} = \frac{\Delta P_{BESS}}{\Delta U} \quad (17)$$

4.1.7. Limiter and Saturation

The energy storage devices are included in the control loop and are regulated by the controller. They have constraints that permit the devices to operate in the nonlinear region. These limitations avert the mechanical shudder because of sudden frequency variations. The constraints are given by

$$\left| \dot{P}_{FESS} < 0.09 \right|, \left| \dot{P}_{BESS} < 0.09 \right|, \left| \dot{P}_{DEG} < 0.01 \right|, \left| \dot{P}_{EV} < 0.01 \right|, |P_{FESS} < 0.9|, \\ |P_{BESS} < 0.2|, |P_{EV} < 0.8| \text{ and } 0 \leq P_{DEG} \leq 0.45$$

4.1.8. Electric Vehicle

The figure presentation modeling of EV for frequency control is demonstrated in Figure 3 [40]. The LFC signal ΔU is supplied to the EV for discharging/charging. Parameters $\pm BkW$ signify the battery capacity. The existing battery energy is signified by E that is kept inside the restrictions E_{\max} and E_{\min} presumed as 90% and 60%. K_1 and K_2 are found as $K_1 = E - E_{\max}$, $K_2 = E - E_{\min}$. The stored energy part in Figure 3 computes the remaining stored energy [40].

4.1.9. Power System

The input and the output to the power system are the difference in power (ΔP) and (Δf) and is given as:

$$G(s) = \frac{\Delta f}{\Delta P} = \frac{1}{D + sM} \quad (18)$$

Here D characterizes the damping parameter and M means inertia value.

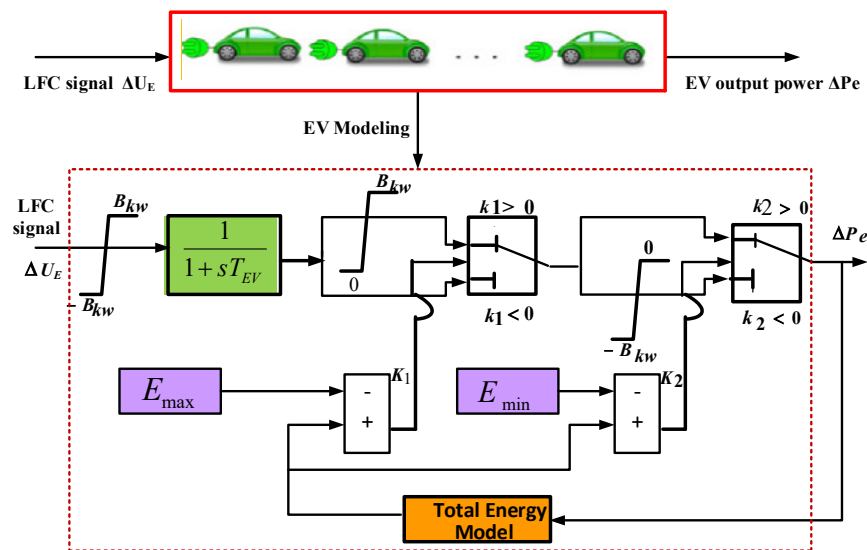


Figure 3. EV Modelling.

4.2. Combined Fuzzy PID Structure

The fuzzy logic control (FLC) based PID controller can be designed by tuning scaling factors and PID parameters [41–45]. In the present work, a combined fuzzy PID (CFPID) is projected as revealed in Figure 4 [45]. To ensure that the controller is adaptive, the input signal is accepted by fuzzy and also straight to the PID as revealed in Figure 5. The membership functions are allocated linguistic PoBg (Positive Big), PoSm (Positive Small), Ze (Zero), NeSm (Negative Small), and NeBg (Negative Big) for inputs/output variables as shown in Table 5. A Mamdani fuzzy inference engine is used in the present study.

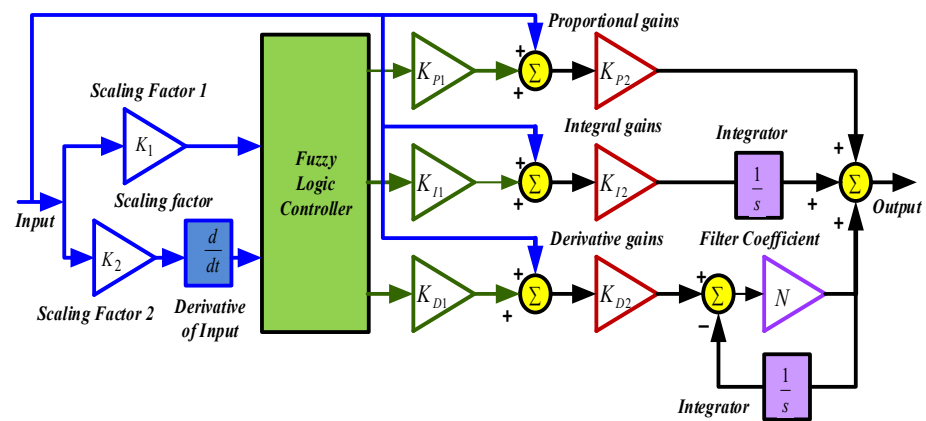


Figure 4. Combined fuzzy PID controller.

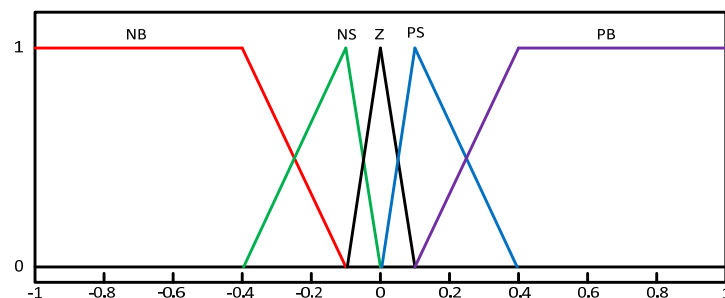


Figure 5. MFs of error and change of error of CFPID.

Table 5. Fuzzy rule foundation for CFPID.

ede	NeBg	NeSm	Ze	PoSm	PoBg
NeBg	NeBg	NeBg	NeSm	NeSm	Ze
NeSm	NeBg	NS	NeSm	PoSm	PoSm
Ze	NeSm	NeSm	Ze	PoSm	PoSm
PoSm	NeSm	Ze	PoSm	PoSm	PoBg
PoBg	Ze	PoSm	PoSm	PoBg	PoBg

An integral square error (ISE) criterion is taken as an objective function as:

$$J = \int_0^T [(\Delta f)^2 + (\Delta U)^2/kn] \cdot dt \quad (19)$$

To ensure that both terms in Equation (19) participate in the search technique, kn is allocated 5.

5. Results and Discussions

5.1. Performance Examination of Proposed Frequency Control Approach

The effectiveness of the recommended ESSA tuned CFPID structure for frequency control is examined in two widely employed 2-area power systems [46–52]. The first test system is a non-reheat system and the second test system is a reheat system. For a fair comparison with published frequency control approaches, the same load disturbance (10% SLP for the first test system and 1% SLP for the second test system) and objective function (ITAE) are considered. In addition, two similar CFPID controllers are assumed in each area. The ESSA optimized CFPID controller parameters are provided in Table 6. The results of the proposed controller are related to traditional as well as numerous new optimization techniques, for example, Ziegler Nichols (ZN) [46], GA [46], BFOA [46], PSO [47], hybrid BFOA-PSO [47], NSGA-II based PI [48], NSGA-II optimized PIDF [48], hybrid PSO-PS optimized fuzzy PI [43] as well as mMSA Fuzzy PD-PI [37] for the first test system and shown in Table 7 and Figure 6 for the first test system.

Table 6. Optimized parameters for two test systems.

1st test system	$K_1 = 1.9847, K_2 = 0.5802, K_{P1} = 1.7138, K_{I1} = 1.9742, K_{D1} = 0.2796, K_{P2} = 1.4912, K_{I2} = 1.9966, K_{D2} = 0.2249$
2nd test system	$K_1 = 1.9847, K_2 = 1.9867, K_{P1} = 1.9959, K_{I1} = 1.9742, K_{D1} = 0.002, K_{P2} = 1.9965, K_{I2} = 1.9966, K_{D2} = 0.0999$

Table 7. Performance with different controllers for 1st test system.

Method/Controller	ITAE	Settling Time (T_s) S			Undershoot (Us)-ve		
		Δf_1	Δf_2	ΔP_{tie}	Δf_1	Δf_2	ΔP_{tie}
GA: PI [46]	2.7475	10.3	10.3	9.3	0.23	0.19	0.07
BFOA: PI [46]	1.8379	7.1	5.5	6.35	0.27	0.23	0.08
hBFOA-PSO-PI [47]	1.1865	6.6	6.2	5.73	0.24	0.21	0.071
NSGA-II: PIDF [48]	0.387	4.86	3.03	4.34	0.103	0.052	0.023
hPSO-PS-Fuzzy PI [43]	0.1438	5.25	4.07	4.01	0.07	0.035	0.012
mMSA: Fuzzy PD-PI [37]	0.1783	2.71	4.29	3.95	0.052	0.038	0.011
Proposed ESSA based CFPID	0.0262	1.21	1.05	1.02	0.0483	0.0167	0.0058

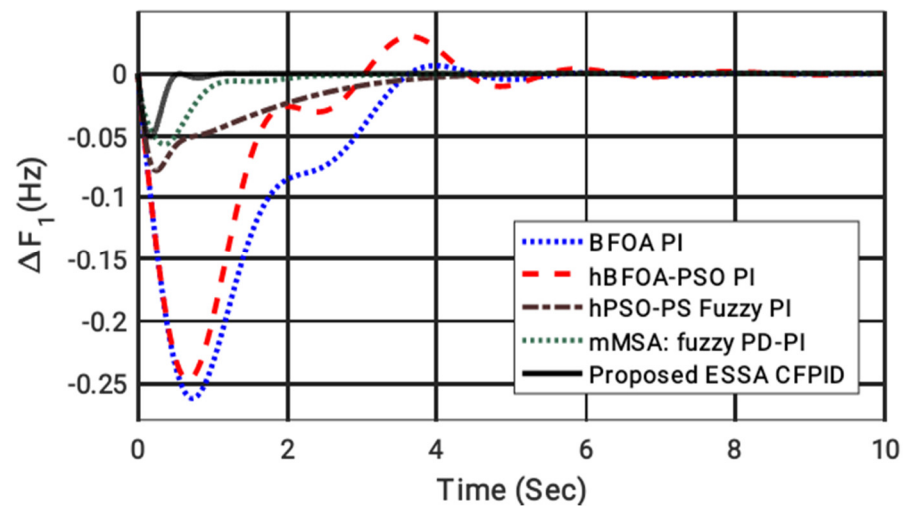


Figure 6. Frequency deviation of first area for 1st test system.

It is obvious from Table 7 and Figure 6 that the least ITAE value and best system response are attained with an ESSA-based CFPID controller compared to other approaches usually used in solar electricity control [49]. For the second test system, the results are compared FA [50], SOSA [51], ABC [52] tuned PID and SGWO tuned AFPID [39]. The outcomes are gathered in Table 8 and Figure 7. The minimum ITAE value and best system response are attained with ESSA-based CFPID controller compared to other approaches as evident from Table 8 and Figure 7. This justifies the usefulness of the proposed CFPID controller structure.

Table 8. Objective function values for the different controllers for 2nd test system.

Technique: Control Structure	ITAE
PID/FA [50]	10.12×10^{-2}
PID/SOSA [51]	9.96×10^{-2}
PID/ABC [52]	5.72×10^{-2}
SGWO: AFPID [53]	2.79×10^{-2}
Proposed ESSA based CFPID	1.34×10^{-2}

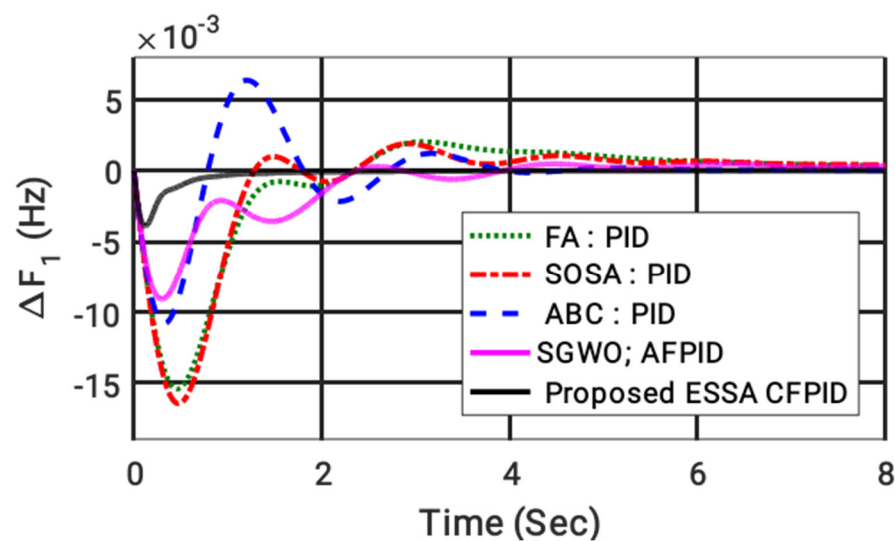


Figure 7. Frequency deviation of first area for 2nd test system.

5.2. Frequency Control of DPGS by PD-CFPID

In the next step, DPS is considered and the controllers are optimized by the ESSA technique. The load demand (P_D) pattern is revealed in Figure 8a. The renewable outputs are characterized by Equations (17)–(19) and adopted from [5,36–39] as presented in Figure 8b,c. Table 8 provides the ESSA optimized PID, CFPID, and PD-CFPID controller parameters. For comparison, the results of MFO, PSO, GA, DA, GSA, and SSA optimized PID and J values are also specified in Table 9 from which it can be seen that, with the same PID controller, a minimum objective function value of 782.75×10^{-2} is obtained with the proposed ESSA technique. Hence, it is established that in the controller design problem, the proposed ESSA outperforms MFO, PSO, GA, DA, GSA, and SSA techniques. The CFPID controller optimized by ESSA reduces the J value to 781.99×10^{-2} . This validates the dominance of the CFPID over the PID. It can also be understood from Table 9 that the suggested PD-CFPID controller significantly reduces the J value to 368.31×10^{-2} .

Table 9. Optimized values.

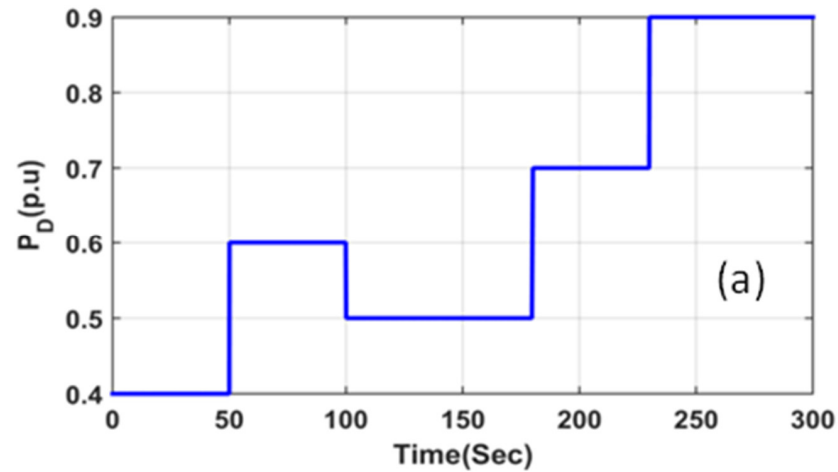
Technique	Optimized Parameters			J Value ($\times 10^{-2}$)
	PID			
	K_P	K_I	K_D	
MFO	0.5919	0.3137	1.1244	789.15
PSO	0.6370	0.3719	1.3587	789.05
GA	0.6016	0.3106	1.0199	788.89
DA	0.6716	0.3685	1.2448	788.97
GSA	0.6484	0.3550	1.5325	787.62
SSA	0.7106	0.2211	1.0787	783.20
ESSA	0.7172	0.2489	1.0371	782.75
	CFPID			
ESSA: CFPID	$K_1 = 1.3967, K_2 = 1.5397$ $K_{P1} = 1.5495, K_{I1} = 1.5744, K_{D1} = 0.8160$ $K_{P2} = 0.2288, K_{I2} = 0.7581, K_{D2} = 1.3056$			781.99
ESSA: PD-CFPID	$K_1 = 1.4319, K_2 = 0.8438$ $K_{P1} = 1.5183, K_{I1} = 1.9570, K_{D1} = 1.9764$ $K_{P2} = 0.1992, K_{I2} = 0.6637, K_{D2} = 1.9570$ CPF-FESS = 1.9564; CPF-BESS = 1.7787 CPF-DEG = 1.9987; CPF-EV = 1.7965			368.31

To assess the controller's effectiveness, the following cases are taken.

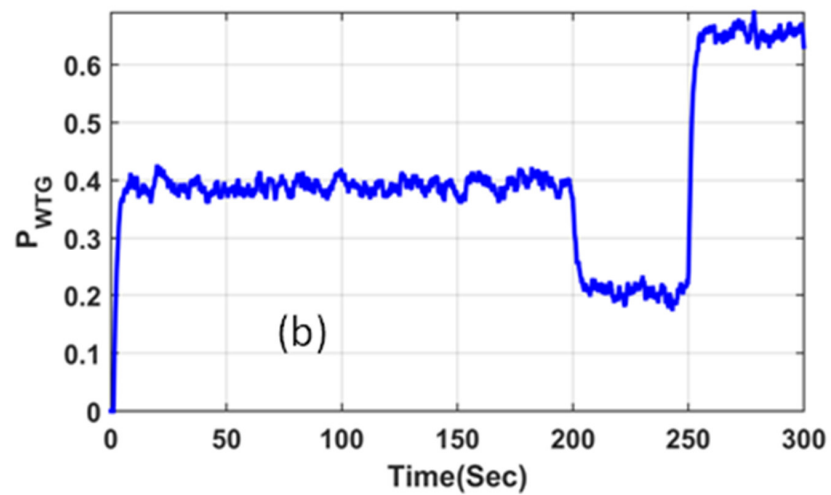
Case 1: Normal operation:

Here, solar and wind generation and load outlines as specified in Figure 8 are presumed. The dynamic response with ESSA-based PID, CFPID, and PD-CFPID is presented in Figure 9. It is clear from Figure 9a that the performance with PD-CFPID is slightly better than PID and CFPID. The power outputs with the proposed PD-CFPID controller are shown in Figure 9b,c. In the time range $t = 50$ to 100 s it can be seen from Figure 8a that P_D is 0.6 pu. The P_{WTG} is around 0.4 p.u., P_{PV} is 0.2 pu which is clear from Figure 8b,c. Aqua electrolyzer takes 0.24 p.u. from the generation of renewable sources used by a fuel cell and the fuel cell gives a power that is equal to 0.0001 pu. DEG also becomes coupled to DPS at $t = 50$ s and supplies a power equal to 0.007 p.u. which is revealed in Figure 9b. The whole generation is obtained by totaling the power generation from the renewable sources less the aqua electrolyzer power, and by adding the power from DEG the fuel cell becomes 0.367 p.u. This is 0.23 p.u. less than P_D so BESS, FESS, and electric vehicles (EV) deliver less power to meet P_D . $P_{FESS} = 0.0075$ p.u., $P_{BESS} = 0.0022$ p.u., $P_{PEV} = 0.23$ p.u. which are exhibited in Figure 9b,c. When the power is released by the storage devices and

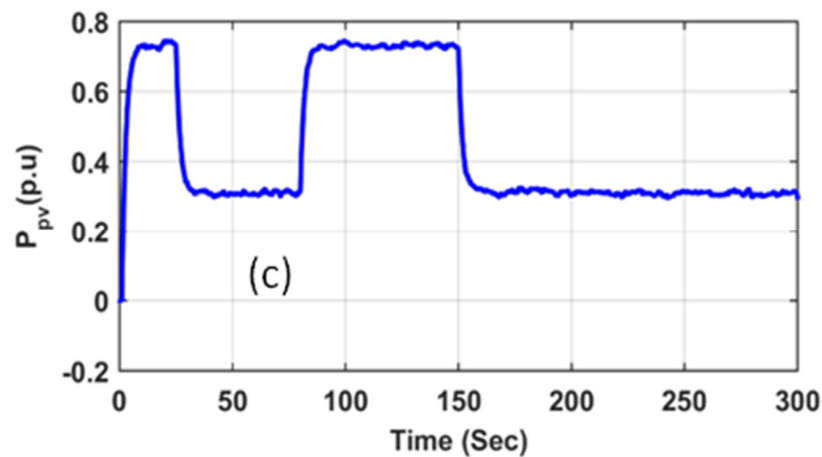
power discharged by P_{ev} is added to the generated power, the supply power becomes 0.6 p.u., which is the same as P_D . Hence, the power balance is maintained and the system is frequently stable.



(a) Load demand



(b) Wind power



(c) Solar power

Figure 8. (a) P_D (b) P_{WTG} (c) P_{PV} (independent controller).

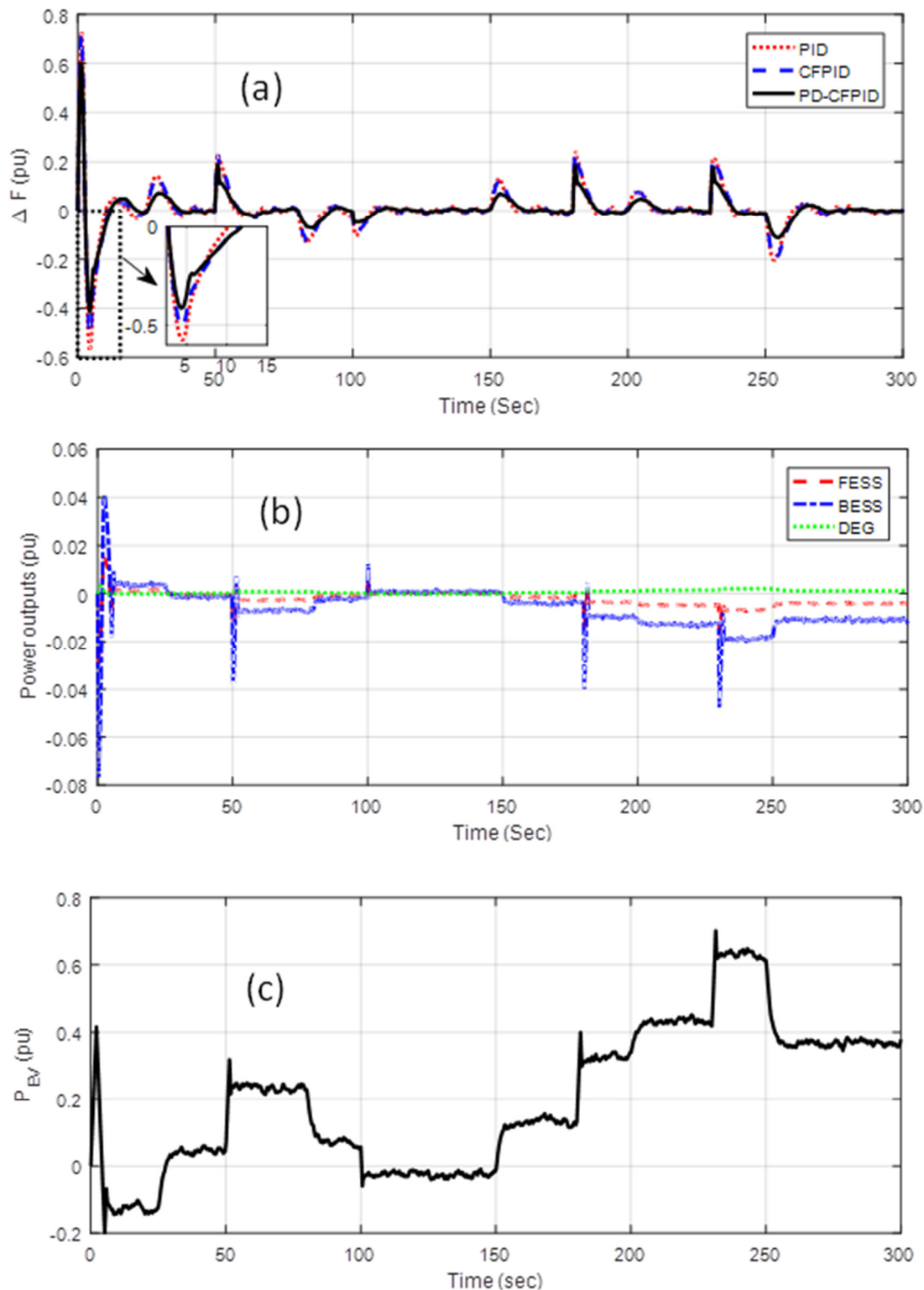


Figure 9. System response for case 1 (a) ΔF . (b) P_{BESS} , P_{FESS} and P_{DEG} . (c) P_{EV} .

Case 2: Uncertain Cases

The renewable sources are associated with uncertainty and so is the case with load demand and EV. Keeping in view of some realistic variation/uncertainties, different cases are considered. To prove the supremacy of suggested PD-CFPID over CFPID and PID, the

responses with PD-CFPID are compared with CFPID and PID under various uncertain conditions as:

Scenario A: P_{WTG} , P_{PV} , and P_D are augmented by 200%;

Scenario B: P_{WTG} and P_{PV} are unavailable but the P_D is augmented by 200%;

Scenario C: EV power and load demand pattern are augmented by 100% and 200%, respectively;

Scenario B: P_{WTG} and P_{PV} are decreased by 50% but P_{EV} and P_D are augmented by 100% and 200%, respectively;

Scenario E: The time delay is enhanced to 400 ms.

The responses for the above situations are presented in Figure 10a–e. It can be comprehended from Figure 10a that, for scenario A, when solar, wind powers, and load demand patterns are increased by 200%, the system is unstable with the PID. System stability is preserved with both CFPID and PD-CFPID. However, the response degrades with CFPID under scenario A whereas the response remains unaffected with the proposed PD-CFPID controller. For scenario B, when P_{WTG} and P_{PV} are unavailable but the P_D is augmented by 200%, the system is unstable with PID. The response further degrades with the CFPID controller in scenario B compared to the same for scenario A. with the proposed PD-CFPID controller, the response remains more or less the same. For scenarios C, D, and E, the system is unstable with both PID and CFPID controllers as evident from Figure 10c–e. However, the system stability is retained with the suggested PD-CFPID controller and frequency deviations lie inside the acceptable boundary.

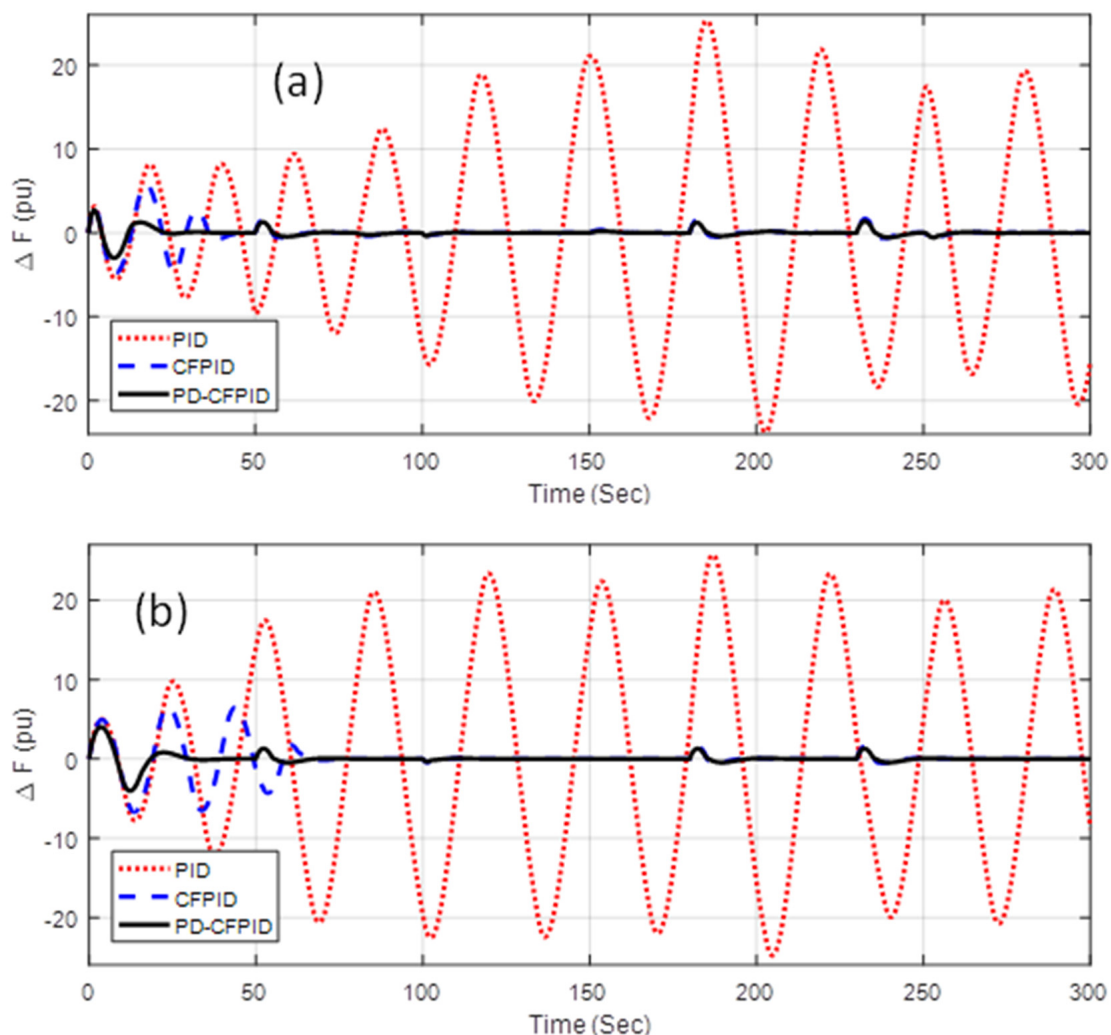


Figure 10. Cont.

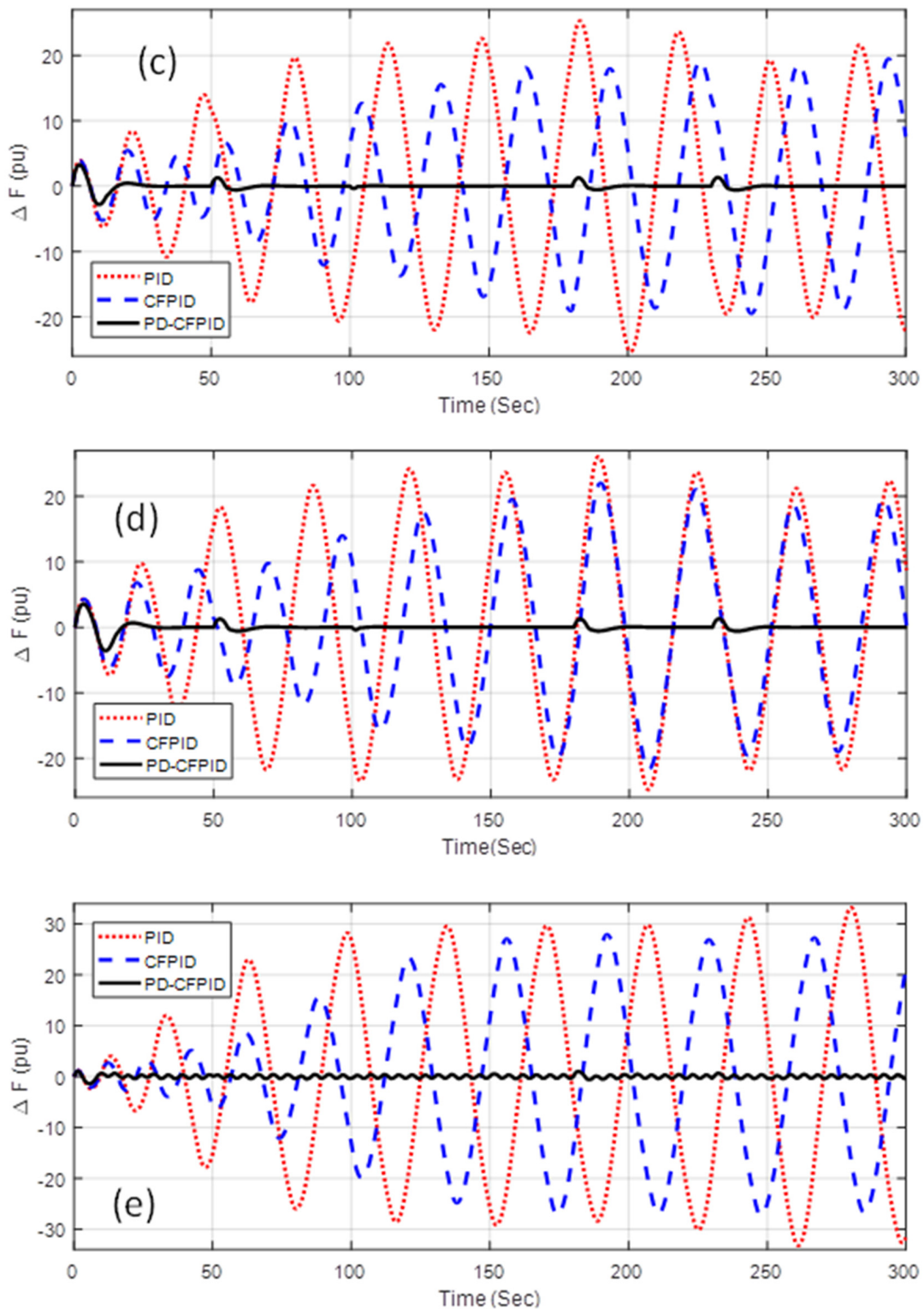


Figure 10. System response under uncertain cases. (a) System response for scenario A. (b) System response for scenario B. (c) System response for scenario C. (d) System response for scenario D. (e) System response for scenario E.

In the present study, only multimodal functions have been tested as the controller design problem is a multimodal task. The usefulness of the proposed MSSA for unimodal functions and other benchmark functions needs further investigation.

6. Conclusions

In this paper, the enhanced salp swarm algorithm (ESSA) method was presented for solving multimodal optimization and controller design. In the suggested ESSA method, the convergence parameter is varied suitably for an improved equilibrium among the exploration and exploitation stages of the technique. Additionally, variable scaling factors are engaged to alter the salp's position in the search procedure to minimize the random movement of salps. The effectiveness of ESSA is confirmed in some multimodal test functions. It is seen that for 10-dimensional multimodal functions (*mmfs'*), the ESSA algorithm provides improved results more than SSA, GA, ABC, CamWOA, MFO, PSO, GSA, WCA, PSOGSA, DA, and WCMFO in four out of six *mmfs'*. For fixed dimension *mmfs'*, proposed ESSA provides optimum or equally best outcomes in nine out of ten *mmfs'*. The projected control method is evaluated in two widely used systems. It is detected that the *J* value is reduced by 81.78% and 76.57% related to the best-published results for the two test systems, respectively.

The proposed ESSA method is then used to optimize a partially decentralized combined fuzzy PID (PD-CFPID) controller for frequency control of DPS. It is perceived that the ESSA-based PD-CFPID controller is better than PID and CFPID controllers and maintains frequency stability under various uncertain scenarios. The objective function value with the PD-CFPID controller is reduced by 52.94% and 52.90% compared to PID and CFPID controllers.

As a future direction, experimental verification of the present work can be performed and the state of charge of EVs can be included in the system.

Author Contributions: Conceptualization, S.N., S.K.K. and S.S.D.; methodology, S.N., S.K.K. and P.V.; software, P.V. and S.B.T.; validation, S.N., S.K.K. and P.V.; formal analysis, S.B.T. and B.N.; investigation, S.N., S.K.K. and P.V.; resources, S.B.T. and B.N.; data curation, S.N., S.K.K. and P.V.; writing—original draft preparation, P.S.N., S.K.K. and S.S.D.; writing—review and editing, P.V., S.B.T. and B.N.; visualization, S.N. and P.V.; supervision, P.V., S.B.T. and B.N.; project administration, S.B.T. and B.N.; funding acquisition, S.B.T. and B.N. All authors have read and agreed to the published version of the manuscript.

Funding: This research received no external funding.

Conflicts of Interest: The authors declare no conflict of interest.

References

1. Lee, D.-J.; Wang, L. Small-Signal Stability Analysis of an Autonomous Hybrid Renewable Energy Power Generation/Energy Storage System Part I: Time-Domain Simulations. *IEEE Trans. Energy Convers.* **2008**, *23*, 311–320. [[CrossRef](#)]
2. Yang, H.; Chung, C.Y.; Zhao, J. Application of plug-in electric vehicles to frequency regulation based on distributed signal acquisition via limited communication. *IEEE Trans. Power Syst.* **2013**, *28*, 1017–1026. [[CrossRef](#)]
3. Savino, M.M.; Manzini, R.; Della Selva, V.; Accorsi, R. A new model for environmental and economic evaluation of renewable energy systems: The case of wind turbines. *Appl. Energy* **2017**, *189*, 739–752. [[CrossRef](#)]
4. Benavente, I.M.; Lazaro, E.G.; Sanchez, T.G.; Rodríguez, A.V.; Garcia, A.M. Implementation and assessment of a decentralized load frequency control: Application to power systems with high wind energy penetration. *Energies* **2017**, *10*, 151. [[CrossRef](#)]
5. Pan, I.; Das, S. Fractional Order AGC for Distributed Energy Resources Using Robust Optimization. *IEEE Trans. Smart Grid* **2015**, *7*, 2175–2186. [[CrossRef](#)]
6. Mirjalili, S.; Gandomi, H.; Mirjalili, S.; Saremi, S.; Faris, H.; Mirjalili, S.M. Salp swarm algorithm: A bio-inspired optimizer for engineering design problems. *Adv. Eng. Softw.* **2017**, *114*, 163–191. [[CrossRef](#)]
7. Guha, D.; Roy, P.K.; Banerjee, S. Quasi-oppositional JAYA optimized 2-degree-of-freedom PID controller for load-frequency control of interconnected power systems. *Int. J. Model. Simul.* **2020**, *42*, 63–85. [[CrossRef](#)]
8. Khokhar, B.; Dahiya, S.; Parmar, K.S. Load frequency control of a microgrid employing a 2D Sine Logistic map based chaotic sine cosine algorithm. *Appl. Soft Comput.* **2021**, *109*, 107564. [[CrossRef](#)]
9. Khokhar, B.; Parmar, K.P.S. A novel adaptive intelligent MPC scheme for frequency stabilization of amicrogrid considering SoC control of EVs. *Appl. Energy* **2021**, *309*, 118423. [[CrossRef](#)]
10. Peddakapu, K.; Mohameda, M.R.; Srinivasarao, P.; Leung, P.K. Frequency stabilization in interconnected power system using bat and harmony search algorithm with coordinated controllers. *Appl. Soft Comput.* **2021**, *113*, 107986. [[CrossRef](#)]
11. El-Ela, A.A.A.; El-Sehiemy, R.A.; Shaheen, A.M.; Diab, A.E.-G. Design of cascaded controller based on coyote optimizer for load frequency control in multi-area power systems with renewable sources. *Control Eng. Pract.* **2022**, *121*, 105058. [[CrossRef](#)]

12. Irudayaraj, A.X.R.; Wahab, N.I.A.; Premkumar, M.; Radzi, M.A.M.; Bin Sulaiman, N.; Veerasamy, V.; Farade, R.A.; Islam, M.Z. Renewable sources-based automatic load frequency control of interconnected systems using chaotic atom search optimization. *Appl. Soft Comput.* **2022**, *119*, 108574. [[CrossRef](#)]
13. Rai, A.; Das, D.K. The development of a fuzzy tilt integral derivative controller based on the sailfish optimizer to solve load frequency control in a microgrid, incorporating energy storage systems. *J. Energy Storage* **2022**, *48*, 103887. [[CrossRef](#)]
14. Shayeghi, H.; Rahnama, A.; Alhelou, H. Frequency control of fully-renewable interconnected microgrid using fuzzy cascade controller with demand response program considering. *Energy Rep.* **2021**, *7*, 6077–6094. [[CrossRef](#)]
15. Kumar, A.; Pan, S. Design of fractional order PID controller for load frequency control system with communication delay. *ISA Trans.* **2021**, *in press*. [[CrossRef](#)]
16. Irudayaraj, A.X.R.; Wahab, N.I.A.; Umamaheswari, M.G.; Radzi, M.A.M.; Bin Sulaiman, N.; Veerasamy, V.; Prasanna, S.C.; Ramachandran, R. A Matignon's Theorem Based Stability Analysis of Hybrid Power System for Automatic Load Frequency Control Using Atom Search Optimized FOPID Controller. *IEEE Access* **2020**, *8*, 168751–168772. [[CrossRef](#)]
17. Padhy, S.; Panda, S. Application of a simplified Grey Wolf optimization technique for adaptive fuzzy PID controller design for frequency regulation of a distributed power generation system. *Prot. Control Mod. Power Syst.* **2021**, *6*, 2. [[CrossRef](#)]
18. Patel, N.C.; Sahu, B.K.; Bagarty, D.P.; Das, P.; Debnath, M.K. A novel application of ALO-based fractional order fuzzy PID controller for AGC of power system with diverse sources of generation. *Int. J. Electr. Eng. Educ.* **2021**, *58*, 465–487. [[CrossRef](#)]
19. Al-Hinai, A.; Alyammahi, H.; Alhelou, H.H. Coordinated intelligent frequency control incorporating battery energy storage system, minimum variable contribution of demand response, and variable load damping coefficient in isolated power systems. *Energy Rep.* **2021**, *7*, 8030–8041. [[CrossRef](#)]
20. Ahmed, M.; Magdy, G.; Khamies, M.; Kamel, S. Modified TID controller for load frequency control of a two-area interconnected diverse-unit power system. *Int. J. Electr. Power Energy Syst.* **2022**, *135*, 107528. [[CrossRef](#)]
21. Sobhy, M.A.; Abdelaziz, A.Y.; Hasanien, H.M.; Ezzat, M. Marine predators algorithm for load frequency control of modern interconnected power systems including renewable energy sources and energy storage units. *Ain. Shams Eng. J.* **2021**, *12*, 3843–3857. [[CrossRef](#)]
22. Weldcherkos, T.; Salau, A.O.; Ashagrie, A. Modeling and design of an automatic generation control for hydropower plants using Neuro-Fuzzy controller. *Energy Rep.* **2021**, *7*, 6626–6637. [[CrossRef](#)]
23. Taghvaei, M.; Gilvanejad, M.; Sedighizade, M. Cooperation of large-scale wind farm and battery storage in frequency control: An optimal Fuzzy-logic based controller. *J. Energy Storage* **2022**, *46*, 103834. [[CrossRef](#)]
24. Khalilpourazari, S.; Khalilpourazary, S. An efficient hybrid algorithm based on Water Cycle and Moth-Flame Optimization algorithms for solving numerical and constrained engineering optimization problems. *Soft Comput.* **2019**, *23*, 1699–1722. [[CrossRef](#)]
25. Karaboga, D.; Basturk, B. A powerful and efficient algorithm for numerical function optimization: Artificial bee colony (ABC) algorithm. *J. Glob. Optim.* **2007**, *39*, 459–471. [[CrossRef](#)]
26. Holland, J.H. Genetic algorithms. *Sci. Am.* **1992**, *267*, 66–72. [[CrossRef](#)]
27. Saha, N.; Panda, S. Cosine adapted modified whale optimization algorithm for control of switched reluctance motor. *Comput. Intell.* **2020**. [[CrossRef](#)]
28. Kennedy, J.; Eberhart, R. Particle Swarm Optimization. In Proceedings of the IEEE International Conference on Neural Networks, Perth, Australia, 27 November–1 December 1995; pp. 1942–1948.
29. Rashedi, E.; Nezamabadi-Pour, H.; Saryazdi, S. GSA: A Gravitational Search Algorithm. *Inf. Sci.* **2009**, *179*, 2232–2248. [[CrossRef](#)]
30. Mirjalili, S.; Hashim, S.Z.M. A new hybrid PSO-GSA algorithm for function optimization. In Proceedings of the 2010 International Conference on Computer and Information Application (ICCIA), Tianjin, China, 3–5 December 2010; Volume 3, pp. 374–377.
31. Eskandar, H.; Sadollah, A.; Bahreininejad, A.; Hamdi, M. Water cycle algorithm—A novel metaheuristic optimization method for solving constrained engineering optimization problems. *Comput. Struct.* **2021**, *110*, 151–166. [[CrossRef](#)]
32. Mirjalili, S. Moth-flame optimization algorithm: A novel nature-inspired heuristic paradigm. *Knowl. Based Syst.* **2015**, *89*, 228–249. [[CrossRef](#)]
33. Mirjalili, S. Dragon fly algorithm: A new meta-heuristic optimization technique for solving single-objective, discrete and multi-objective problems. *Neural Comput. Appl.* **2016**, *27*, 1053–1073. [[CrossRef](#)]
34. Digalakis, J.; Margaritis, K. On benchmarking functions for genetic algorithms. *Int. J. Comput. Math.* **2001**, *77*, 481–506. [[CrossRef](#)]
35. Yao, X.; Liu, Y.; Lin, G. Evolutionary programming made faster. *IEEE Trans. Evol. Comput.* **1999**, *3*, 82–102. [[CrossRef](#)]
36. Rajesh, K.S.; Dash, S.S. Load frequency control of autonomous power system using adaptive fuzzy based PID controller optimized on improved sine cosine algorithm. *J. Ambient. Intell. Humaniz. Comput.* **2019**, *10*, 2361–2373. [[CrossRef](#)]
37. Khamari, D.; Sahu, R.K.; Panda, S. A Modified Moth Swarm Algorithm-Based Hybrid Fuzzy PD–PI Controller for Frequency Regulation of Distributed Power Generation System with Electric Vehicle. *J. Control Autom. Electr. Syst.* **2020**, *1*, 675–692. [[CrossRef](#)]
38. Sivalingam, R.; Chinnamuthu, S.; Dash, S.S. A modified whale optimization algorithm-based adaptive fuzzy logic PID controller for load frequency control of autonomous power generation systems. *Automatica* **2018**, *58*, 410–421. [[CrossRef](#)]
39. Mohanty, D.; Panda, S. Frequency control of hybrid power system by sine function adapted improved whale optimisation technique. *Int. J. Ambient. Energy* **2020**. [[CrossRef](#)]

40. Padhy, S.; Panda, S.; Mahapatra, S. A modified GWO technique based cascade PI-PD controller for AGC of power systems in presence of Plug in Electric Vehicles. *Eng. Sci. Technol. Int. J.* **2017**, *20*, 427–442. [[CrossRef](#)]
41. Savran, A.; Kahraman, G. A fuzzy model based adaptive PID controller design for nonlinear and uncertain processes. *ISA Trans.* **2014**, *53*, 280–288. [[CrossRef](#)]
42. Woo, Z.-W.; Chung, H.-Y.; Lin, J.-J. A PID type fuzzy controller with self-tuning scaling factors. *Fuzzy Sets Syst.* **2000**, *115*, 321–326. [[CrossRef](#)]
43. Sahu, R.K.; Panda, S.; Sekhar, G.C. A novel hybrid PSO-PS optimized fuzzy PI controller for AGC in multi area interconnected power systems. *Int. J. Electr. Power Energy Syst.* **2015**, *64*, 880–893. [[CrossRef](#)]
44. Mohanty, P.K.; Sahu, B.K.; Pati, T.K.; Panda, S.; Kar, S.K. Design and analysis of fuzzy PID controller with derivative filter for AGC in multi-area interconnected power system. *IET Gener. Transm. Distrib.* **2016**, *10*, 3764–3776. [[CrossRef](#)]
45. Fereidouni, A.; Masoum, M.A.; Moghbel, M. A new adaptive configuration of PID type fuzzy logic controller. *ISA Trans.* **2015**, *56*, 222–240. [[CrossRef](#)] [[PubMed](#)]
46. Ali, E.; Abd-Elazim, S. Bacteria foraging optimization algorithm based load frequency controller for interconnected power system. *Int. J. Electr. Power Energy Syst.* **2011**, *33*, 633–638. [[CrossRef](#)]
47. Panda, S.; Mohanty, B.; Hota, P.K. Hybrid BFOA–PSO algorithm for automatic generation control of linear and nonlinear interconnected power systems. *Appl. Soft Comput.* **2013**, *13*, 4718–4730. [[CrossRef](#)]
48. Panda, S.; Yegireddy, N.K. Automatic generation control of multi-area power system using multi-objective non-dominated sorting genetic algorithm-II. *Int. J. Electr. Power Energy Syst.* **2013**, *53*, 54–63. [[CrossRef](#)]
49. Mancini, F.; Nastasi, B. Solar Energy Data Analytics: PV Deployment and Land Use. *Energies* **2020**, *13*, 417. [[CrossRef](#)]
50. Gorripotu, T.S.; Sahu, R.K.; Panda, S. Comparative Performance Analysis of CLASSICAL controllers in LFC Using FA Technique. In Proceedings of the 2015 International Conference on Electrical, Electronics, Signals, Communication and Optimization (EESCO), Visakhapatnam, India, 24–25 January 2015; pp. 1–5.
51. Guha, D.; Roy, P.; Banerjee, S. Symbiotic organism search algorithm applied to load frequency control of multi-area power system. *Energy Syst.* **2018**, *9*, 439–468. [[CrossRef](#)]
52. Gozde, H.; Taplamacioglu, M.C.; Kocaarslan, I. Comparative performance analysis of Artificial Bee Colony algorithm in automatic generation control for interconnected reheat thermal power system. *Int. J. Electr. Power Energy Syst.* **2012**, *42*, 167–178. [[CrossRef](#)]
53. Padhy, S.; Panda, S. Simplified grey wolf optimisation algorithm tuned adaptive fuzzy PID controller for frequency regulation of interconnected power systems. *Int. J. Ambient. Energy* **2021**. [[CrossRef](#)]